NJC

Accepted Manuscript

This is an *Accepted Manuscript*, which has been through the Royal Society of Chemistry peer review process and has been accepted for publication.

Accepted Manuscripts are published online shortly after acceptance, before technical editing, formatting and proof reading. Using this free service, authors can make their results available to the community, in citable form, before we publish the edited article. We will replace this *Accepted Manuscript* with the edited and formatted *Advance Article* as soon as it is available.

You can find more information about *Accepted Manuscripts* in the Information for Authors.

Please note that technical editing may introduce minor changes to the text and/or graphics, which may alter content. The journal's standard Terms & Conditions and the Ethical guidelines still apply. In no event shall the Royal Society of Chemistry be held responsible for any errors or omissions in this *Accepted Manuscript* or any consequences arising from the use of any information it contains.

ROYAL SOCIETY OF CHEMISTRY

www.rsc.org/njc

Nanocomposite for Detoxification of Drinking Water: Effective and Efficient Removal of Fluoride and Bactericidal Activity†

Ankita Dhillon and Dinesh Kumar*

Abstract

The presence of fluoride and biological toxins in groundwater is a worldwide problem and has drawn immense attention. In this study, we have developed a tri–metal (Fe–Ca–Ce) oxide material for fluoride decontamination and bactericide efficiency. The material has shown excellent fluoride adsorption capacity of 384.6 mg g^{-1} as well as superior bactericidal capacity with value of 30 μg mL^{-1} (IC_{50}). The four isotherms studied indicate that the material preferably followed Freundlich and Dubinin–Radushkevich (D–R) isotherms. The adsorption of fluoride followed pseudo–second–order kinetics. The high cationic nature of developed nanomaterial (pzc = 4.5) significantly enhances their better recognition by the negative *E. coli* bacterial membrane causing extensive leakage of large cytoplasmic protein components for death of bacteria. The material triggered efficient inhibition of the enzyme mitochondrial dehydrogenase of *E. coli* (MTCC 498) bacterium. Student's t–test was performed to evaluate statistical significance to verify bactericidal activities. The field applicability of the developed nanomaterial was validated through column studies in real water samples when other ions are also present in the system.

Introduction

Fluorine is the 13th most abundant element in the earth's crust. Fluorine is found in ground water as fluoride (F^-) ion. When present in low concentration (not less than 0.5 mg L^{-1}), then, it functions as an imperative micronutrient in human body meant for calcification of dental enamel and bone configuration. WHO guidelines recommend an uppermost tolerance limit of 1.5 mg L^{-1} fluoride in drinking water.[1] Enforceable and non–enforceable limit of fluoride in drinking water are 4 mg L^{-1} and 2 mg L^{-1} according to Environmental Protection Agency

*Department of Chemistry, Banasthali University, Rajasthan-304022, India; E-mail: dsbchoudhary2002@gmail.com

†Electronic supplementary information (ESI) available: N_2 Adsorption/Desorption curves, FTIR spectra of adsorbent pre– and post–adsorption, XRD patterns, Langmuir and Temkin isotherm outlines, pseudo–first–order plots, potentiometric titration, and effect of co–existing anions.

(EPA, USA).[2] Maximum contamination level for fluoride in drinking water is 0.7 mg L^{-1} according to the department of human health and services.[4] Main sources of fluoride are various kinds of rocks, soil, plants, animals, humans, and ocean water. Untreated industrial effluents, mining operations, and use of fertilizers also augment fluoride buildup in community and groundwater systems. This, leads to accumulation of fluoride compounds in the surface waters and groundwater sources.[2–4] In one hand, ffluoride contact has a multifaceted connection with dental caries and may augment dental caries threat when present in less amounts.[4] On the other hand, skeletal fluorosis, a chronic metabolic bone disease, paralysis, muscles weakness, stiffness of joints, and chronic fatigue are the other health hazards.[5] Out of 85 million tons, 12 million tons fluoride deposits on the earth's crust are found in India the most affected areas being Uttar Pradesh, Rajasthan, Gujarat, Andhra Pradesh, and Tamil Nadu, where, fluoride is present in elevated concentrations.[6,7] This issue needs to be immediately addressed considering the harmful effects of excess fluoride intake. Consequently, increasing environmental concerns regarding elevated F^- concentration in water have led to the development of defluoridation techniques. A large number of techniques i.e. adsorption,[3] ion exchange,[8] precipitation,[9] Donnan dialysis,[10] electrodialysis,[11] reverse osmosis,[12] nanofiltration,[13] and ultrafiltration[14] have been investigated for the fluoride removal. As compared to other technologies like reverse osmosis,[15] nanofiltration, electrodialysis,[16] and Donnan dialysis,[17] adsorption is considered among the most competent tools for defluoridation of drinking water, and it has been extensively used in detoxicification of water.[18] A variety of adsorbents have been examined for the fluoride remediation, comprising alumina based adsorbents,[19,20] activated carbon,[21] bone char,[22] synthetic ion exchangers,[23] layered double hydroxides,[24] natural materials,[25] chitosan beads,[26,27] clays, and soils.[28,29] Fluoride uptake using calcium based adsorbents has been reported in the past decade.[30–32] Additionally, a range of iron based composite materials,[33–37] and cerium based hybrid materials[38–40] have also been used to treat contaminated water. These materials have shortcomings in regards of low fluoride removal efficiency, cost, and, ecological impact. Hence, to eradicate the demerits of the above three classes of adsorbents, a grouping of iron, calcium and cerium would be expected to be a more robust and competent adsorbent for adsorptive remediation of fluoride. According to safe drinking water act, EPA necessitates community water schemes to check for coliform bacteria. Drinking water contaminated with bacteria especially *E. coli* may result into kidney damage,[41] weakness of small intestinal walls in children, severe anaemia, various urinary tract infections[42] etc. Therefore, removal or inactivation of infectious *E. coli* contaminations from drinking water is also the

prime matter of concern for researchers. Most of the usual disinfection methods for instance chlorination and ozonation are inadequate, and also comprise a number of limitations.[43] Therefore, to overcome these limitations metal oxide nanomaterials have gained much interest as antibacterial agents. To the best of our knowledge, a few materials are known to simultaneously remove fluoride as well as *E. coli* from drinking water.[44–46] The developed nanomaterial in the present study presents an efficient solution for both fluoride removal and exhibited strong inhibitory and bactericidal effects towards *E. coli*.

Experimental Section

Chemicals and Materials

All the chemicals and reagents were procured from Sigma–Aldrich Ltd. and used as received without any further purification. Deionized (DI) water with electrolytic conductivity 0.055 μS/cm was used for the preparation of all aqueous solutions. Glassware was washed with aqua regia and thoroughly rinsed in DI water.

Synthesis of nanomaterial

The tri–metal oxide was synthesized according to previous report.[47] Three metal salt solutions were mixed in equal quotient and the pH of the solution was adjusted ≈ 9.5 by drop–wise addition of 2 M NaOH solution with continuous stirring for precipitation. The precipitate was repeatedly centrifuged and washed at 5000 rpm until the pH of the final solution was 6.3 ± 0.2. Thereafter, precipitate was vacuum dried and then finely powdered. The powder was then activated by slow heating up to 500 ℃ for 6 h in a muffle furnace. The activated nanomaterial was then cooled to room temperature.

Antibacterial Evaluation of Nanomaterial for *E. coli*

Evaluation for IC_{50} of nanomaterial

The strain of *E. coli* (MTCC–498) was purchased from institute of microbial technology, Chandigarh and cultured in Luria Bertani broth (LB broth) for 24 h at 37 ± 1 ℃. To examine the concentration of nanomaterial at which 50% bacterial growth inhibited (IC_{50}), samples having different concentrations of nanomaterial were treated with bacterial sample. For this, a series of culture tubes having 9 mL of LB broth nutrient medium were prepared. To each tube equal volume (0.5 mL) of different concentrations of nanomaterial (10–100 μg mL^{-1}) and 200 μL of bacterial solution were added. The tubes were then incubated for 6 h at 37 ± 1 ℃ for the bacterial growth. All the experiments were performed in triplicates. Eventually, bacterial concentrations in the incubated culture tubes were determined using

spectrophotometer with optical density (OD) at 517 nm. The obtained graphs were compared with those of standard antibiotics (amoxicillin, streptomycin) and IC_{50} values were evaluated.

Statistical analysis

Statistical analysis was performed with SPSSv16.0 (*Predictive Analytics Software*). A set of experiments were carried out three times and mean values and standard deviations were calculated. Student's t–test was performed to evaluate statistical significance. Further p values were computed by the t–test and were considered as significant at 0.05. All the experimental results are presented as means ± SD.

Well diffusion method

To further validate the efficacy of nanomaterial, well diffusion method was also carried out. For this, agar plates in triplicates were prepared with equally spaced bored well. Subsequently, equal amount of 50 μg mL^{-1} and 100 μg mL^{-1} concentration of nanomaterial was added after a single drop of methylene blue dye addition. Finally, the plates were incubated for 24 h at 37 ± 1 ℃ for the development of zone of inhibition.

Evaluation of the effect of nanomaterial on cell membrane leakage in *E. coli*

To determine the effect of nanomaterial on cell wall rupture, the leakage of proteins through membrane was determined. For this, different culture tubes having 5 mL of LB broth and 0.5 mL of different concentrations of nanomaterial (10–100 μg mL^{-1}) and 200 μL of bacterial solutions were added. The tubes were then incubated up to 6 h at 37 ± 1 ℃. One mL culture was collected from the above tubes initially, after 2 h, 4 h, 6 h and centrifuged (12,000 rpm). The freezing of supernatant was carried out at −30 ℃. The concentration of protein was estimated immediately.[48]

Evaluation of enzymatic activity of dehydrogenase in *E. coli*

The effect of nanomaterial on bacterial dehydrogenase enzyme activity was evaluated using MTT (3–(4,5–dimethylthiazol–2–yl)–2,5–diphenyltetrazolium bromide) tetrazolium reduction method. MTT being positively charged and instantly enters viable eukaryotic cells, is used to detect viable cells. The golden yellow colour of the MTT was changed by the enzyme into a purple colored formazan product. Thus, the enzyme activity produced a visual change determined at an absorbance maximum near 570 nm in UV–Vis spectrophotometer. Two different sample tubes having 5 mL of LB broth, 0.5 mL of 50 μg mL^{-1}, 100 μg mL^{-1} concentration of nanomaterial, and 200 μL *E. coli* cells culture were prepared. Tubes devoid of nanomaterial served as the control. Boiled *E. coli* cells (20 min) having completely inactivated enzymes served as the control (−), whereas the unboiled cells having their

enzymes in their native activity served as the control (+). One mL culture was taken out from all the above prepared tubes and centrifuged (12,000 rpm). The pellet was rinsed by phosphate–buffered saline (PBS) and finally suspended in PBS (0.9 mL). MTT solution (0.1 mg mL^{-1}) was added to the prepared samples and then incubated in dark at 37 ± 1 ℃ for 2 h. Subsequently, the reaction was terminated by adding 30 μL of formaldehyde. Finally, the quantity of formazan (most likely relative to the quantity of viable cells) was evaluated by studying absorbance at 570 nm.[49]

Characterization of Nanomaterial

FESEM: The surface microstructure and particle size of developed nanoadsorbent were established by field emission scanning electron microscopy (FESEM, MIRA3 TESCAN). The samples for FESEM were sputtered with Au coating.

EDX: The element composition of adsorbent pre– and post– adsorption was verified by energy dispersive X–ray (EDX) analysis.

FTIR: Vibrational frequencies alterations in functional groups were studied using FTIR analyses with an Agilent 660, USA FTIR spectrophotometer.

XRD: The crystalline structure of nanoadsorbent was illustrated using X–ray diffraction (XRD) patterns. The analysis was carried out using a Bruker D8 Discover X–ray diffractometer with Cu−Kα radiation.

BET: The porosity and surface area characteristics of nanoadsorbent were analysed from N_2 adsorption−desorption isotherms at 77 K. BET parameters were determined using multipoint BET equation (1) given below:[50]

$$\frac{1}{v[\left(\frac{p_o}{p}\right)-1]} = \frac{c-1}{v_m c}\frac{p}{p_o} + \frac{1}{v_m c} \quad (1)$$

where p and p_o are the equilibrium and the saturation pressures of adsorbates at the adsorption temperature, v is the adsorbed gas quantity, c is the BET constant, and v_m is the monolayer gas quantity adsorbed.

Batch adsorption experiments

The adsorption behavior of the developed nanoadsorbent was carried out by batch adsorption studies with various parameters. The effect of pH on the adsorption was studied in a pH range of 2–10. For this, the nanoadsorbent (0.015 g) with synthetic fluoride sample (10 mg L^{-1}) was agitated for 55 min at 150 rpm. Fluoride ion selective electrode (Thermo Scientific Orion, USA) was used for left over fluoride concentration.

Results and Discussion

Surface area and pore characteristics

During analysis in a vacuum degassing mode, 0.40 g of the powdered sample was positioned in the sample cell and allowed to degas for 2 h at 250 ℃. Surface area of adsorbent pre– and post–adsorption obtained (Fig. 1) was 338.9 and 427.4 m^2 g^{-1}, correspondingly. The surface area enhancement exhibits reduction in pore size which evidently illustrates the fluoride adsorption.[50–53] The average D–A pore radius pre– and post–adsorption came out as 15 Å and 13 Å, respectively (Fig. 2). The pore radius was decreased (2 Å) due to the adsorption of fluoride within the pores, ultimately increasing the exterior surface area of the adsorbent whilst it is decreasing interior surface area of pores. Additionally, the porosity was measured in the form of mesopores pre– and post– adsorption, and it had been observed that the porosity as well as pore volume were decreasing upon fluoride adsorption which would be helped to augment surface area of adsorbent (Fig. 2 and Fig. S1†). It is apparent from adsorption capacity results that an extensive fluoride adsorption not only occurred on the exterior adsorbent surface but inside of the pores also. Therefore, the BET surface area of adsorbent is dominated by the surface area of adsorbate.[54] The small size of adsorbate (fluoride) presents high surface area thereby increasing the overall surface area of adsorbent. Additionally, it can also be correlated to the formation of smaller average grain size due to increase in disorder with the adsorption in the host lattice or structural changes occurred due to a chemical reaction.[47,55]

The N_2 adsorption–desorption experiment of nanomaterial exhibited the type IV isotherm associated with the H3 type of hysteresis as shown in Fig. S2†. This type of isotherm also associated with the capillary condensation, takes place in mesopores and initial part of this hysteresis attribute the monolayer and multilayer adsorption. The obtained H3 type of hysteresis strongly favours the presence of mesopores. Furthermore, the closure of isotherm at ~ 0.4 (P/P_0) indicates presence of mesopores and first few multi layers assigned by low slope region in the middle of isotherm.

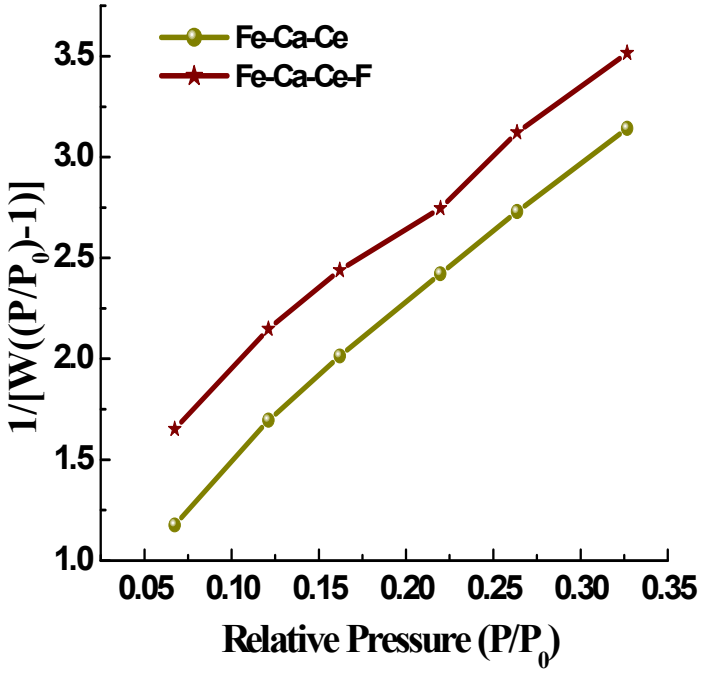

Fig. 1 BET surface area plots.

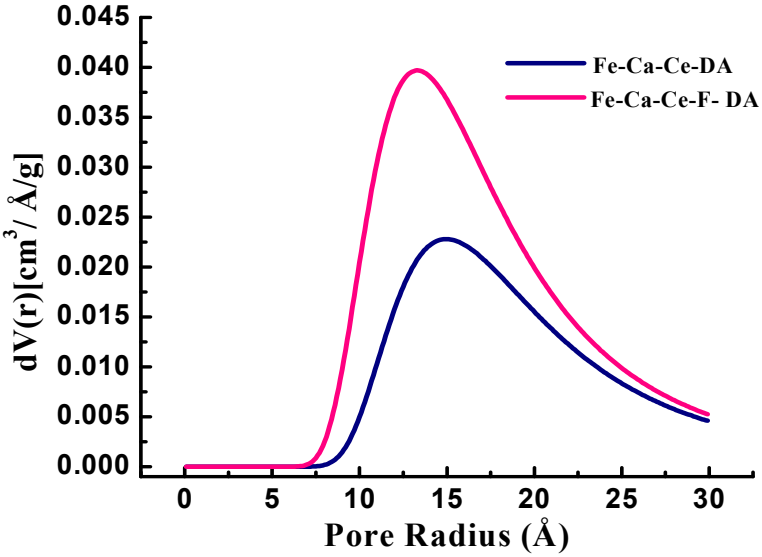

Fig. 2 Pore size distribution of particles calculated using the BET method.

Adsorption mechanism on Fe-Ca-Ce nanoadsorbent

The characteristic peaks at 3476.6 cm^{-1} (broad) and 1648.7 cm^{-1} correspond to the stretching and bending frequencies of OH group of metal hydroxides present in non treated tri–metal

oxide nanoadsorbent (Fig. 3).[52] Furthermore, in fingerprint region two adsorption peaks centered at 1113.0 cm^{-1} and 605.5 cm^{-1} correspond to the bending vibration of MO–H and M–O bond, respectively.[34,53] In confirmation of adsorption, the complete disappearance of the peaks at 1648.7 cm^{-1} and 1113.0 cm^{-1} after fluoride adsorption show the hydroxyl ions are replaced with the fluoride ions during the ion exchange adsorption. Appearance of two new adsorption peaks at 459.6 cm^{-1} and 525.8 cm^{-1} might be due to the Fe–F and Ce–F bond, respectively[56], which is supporting the electrostatic adsorption.

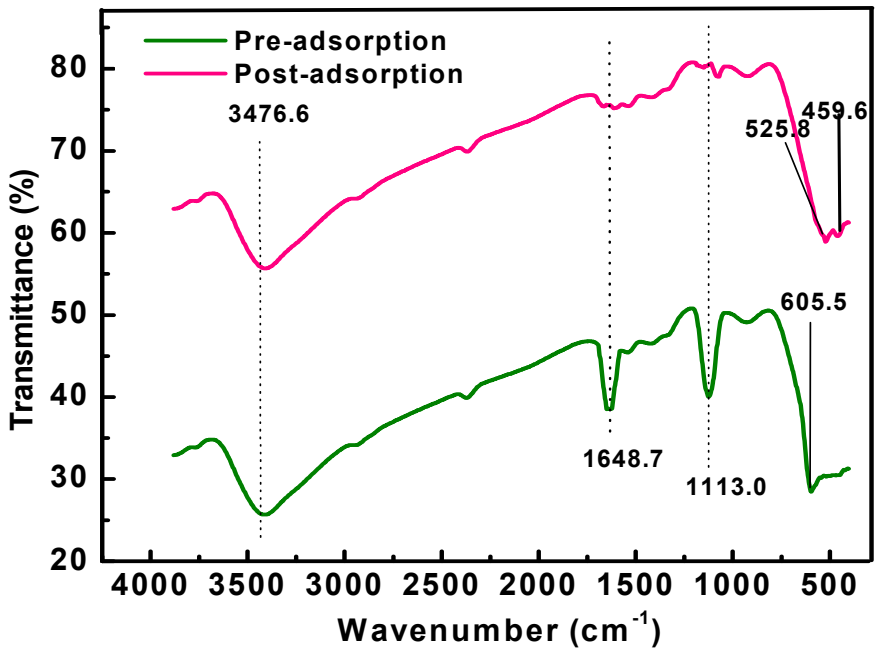

Fig. 3 FTIR spectra of nanoadsorbent (pre– and post–adsorption).

Phase composition

The phase purity and crystallinity of the adsorbent samples (pre– and post– adsorption) were determined by powder X–ray diffraction technique. The broad peaks confirm the nanocrystalline nature of hybrid mesoporous oxide material. The diffraction peaks at 28.57°, 47.60° and 59.13° demonstrate the characteristic peaks of CeO_2.[57] The FeO_2 and CaO_2 phase was hardly detected which may also be due to formation of Fe–Ca–Ce solid solution where the Fe and Ca species has been entered into the lattices of CeO_2. A new characteristic diffraction peak at 20° supports the significant role of cerium in the fluoride adsorption (Fig. S3†).[58,59] Therefore, FTIR and XRD results confirm the stable complexation ability of cerium with fluoride supporting high adsorption capacity.[60]

Surface morphologies and chemical composition

Fig. 4 shows that the particles have non–uniform size with wide size distribution. After fluoride adsorption, the nanoadsorbent has agglomerated in irregular size and shape (Fig 5). The results of EDS mapping confirm the chemical composition of nanoadsorbent as Fe (26.13), Ca (28.64), Ce (14.74) and O (30.45) (Fig. S4†). Further, the adsorption confirms by the presence of the fluoride peak in EDS spectrum (Fig. S5†).

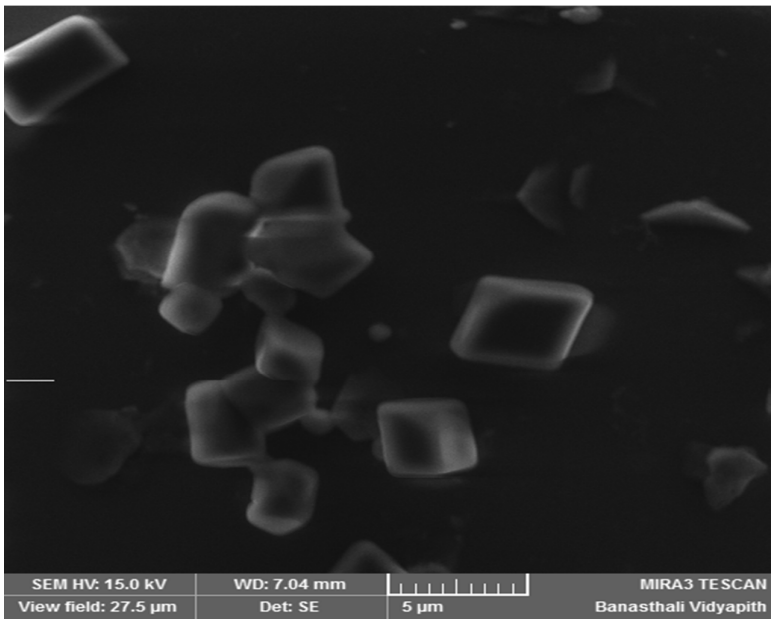

Fig. 4 FESEM image of nanoadsorbent (pre–adsorption).

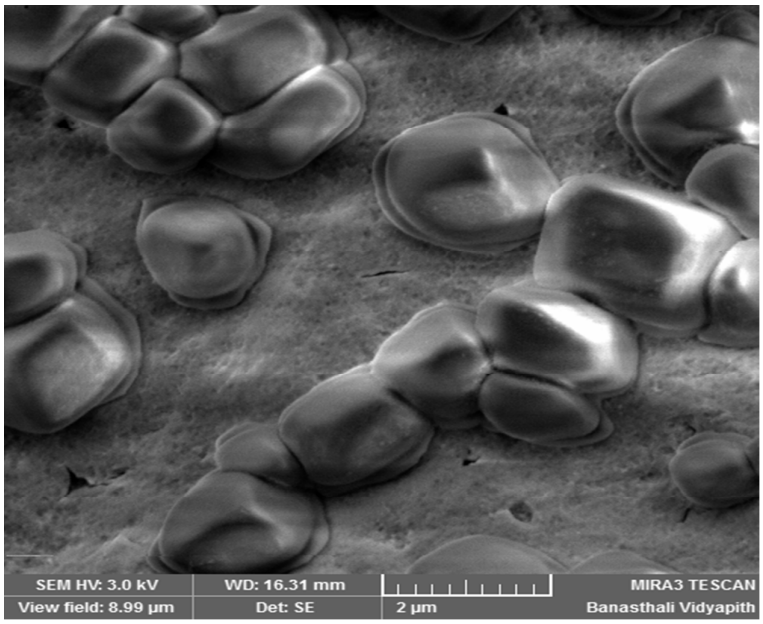

Fig. 5 FESEM image of nanoadsorbent (post–adsorption).

Equilibrium modeling

Adsorption is a separation process in which adsorbate is concentrated from a bulk liquid phase on the surface of solid adsorbent. The most frequently employed isotherms for the application of wastewater treatment are the Freundlich, Langmuir, D–R, and Temkin isotherm. The isotherms experiments were run, and the obtained data were then evaluated by means of the methods that are based on linearization of the models (Table S1†). Among the studied isotherms (Fig. S6†, Fig. S7†, Fig. 6, Fig. 7, and Table S2†), the adsorbent followed well Freundlich and D–R isotherms.

Freundlich isotherm

Multilayer adsorption on the heterogeneous surface sites has been described using Freundlich isotherm model. The isotherm equation and its linear form are expressed in Equations 2 and 3, respectively.

$$q_e = k_F C_e^{1/n} \quad (2)$$

$$\log q_e = \log k_F + 1/n \times \log C_e \quad (3)$$

where Ce is the equilibrium concentration of analyte in solution (mg L^{-1}), k_F is a measure of adsorption capacity, and 1/n is the adsorption intensity. The linear plot of log q_e vs log C_e indicated the applicability the Freundlich isotherm model (Fig. 6).[61] The values of 1/n varied from zero to one whereas the high value of 'n' suggests high removal efficiency, which is validating the favorable adsorption conditions (Table 1).

The Freundlich isotherm having high correlation coefficient R^2 values favour physicochemical nature of adsorption reaction. The k_F values were increasing with temperature that illustrates the temperature dependence of the rate of adsorption reaction.[62]

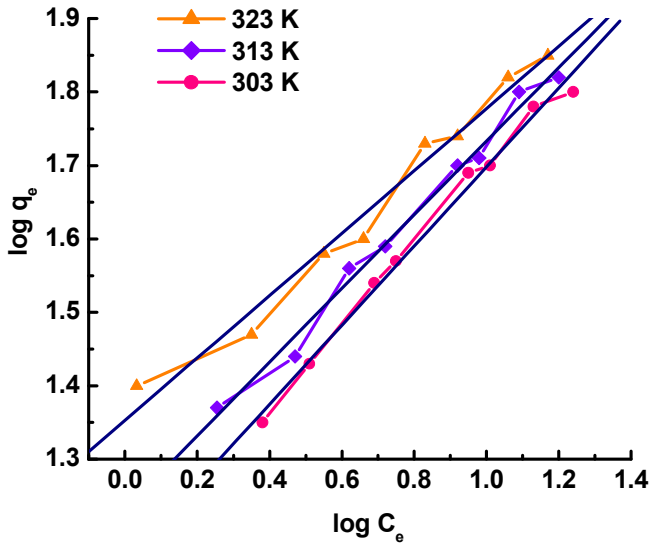

Fig. 6 Freundlich isotherm outlines.

D–R isotherm

The adsorption of fluoride inside the pores and the heterogeneity of the surface energies of adsorption have been described using D–R equation derived from the Polanyi potential theory.[63] The adsorption isotherm equation and its linear form are described in Equations 4 and 5, respectively.

$$q_e = (q_s) \exp(-K_{ad}\, \varepsilon^2) \quad (4)$$

$$\ln(q_e) = \ln(q_s) - (K_{ad}\, \varepsilon^2) \quad (5)$$

where q_s is theoretical isotherm saturation capacity (mg g^{-1}), K_{ad} (mol^2 kJ^{-2}), and ε are D–R isotherm constant (Fig. 7). The value of D–R isotherm constant (K_{ad}) calculated at 303, 313 and 323 K was established to be –0.0147, –0.0154 and —0.0160 mol^2 kJ^{-2}, respectively (Table 1). The mean free energy of adsorption (E) was predicted by means of the relation given below:

$$E = (-2K_{ad})^{-1/2} \quad (6)$$

The calculated energy values are in the range of 8–16 kJ mol^{-1} establishing ion exchange behavior[64] and the energy value increased with temperature. The original Freundlich and Langmuir isotherms are shown in Fig 8.

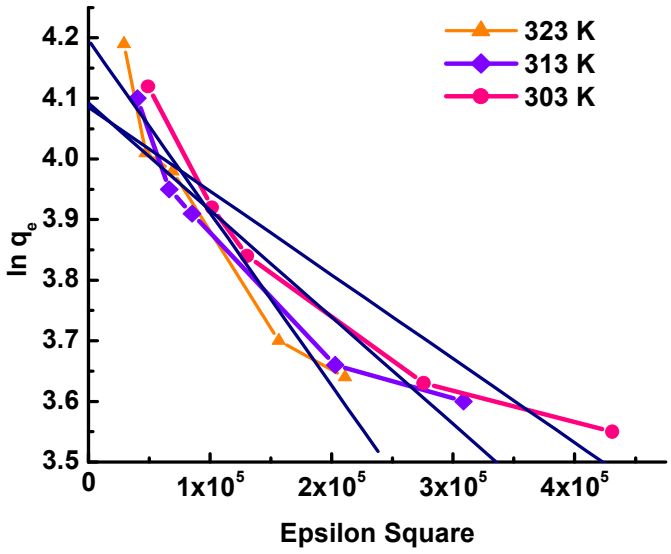

Fig. 7 D–R isotherm outlines.

Table 1 Freundlich and D–R isotherm constants at different temperatures

	D–R isotherm				Freundlich isotherm			
Temperature (K)	K_{ad} (mol^2 kJ^{-2})	q_s (mg g^{-1})	ε	R^2	k_F	1/n	n	R^2
303	–0.0147	4.10	151	0.952	14.5	0.424	2.35	0.981
313	–0.0154	4.10	174	0.973	17.0	0.501	2.00	0.982
323	–0.0160	4.20	151	0.941	22.5	0.540	1.85	0.979

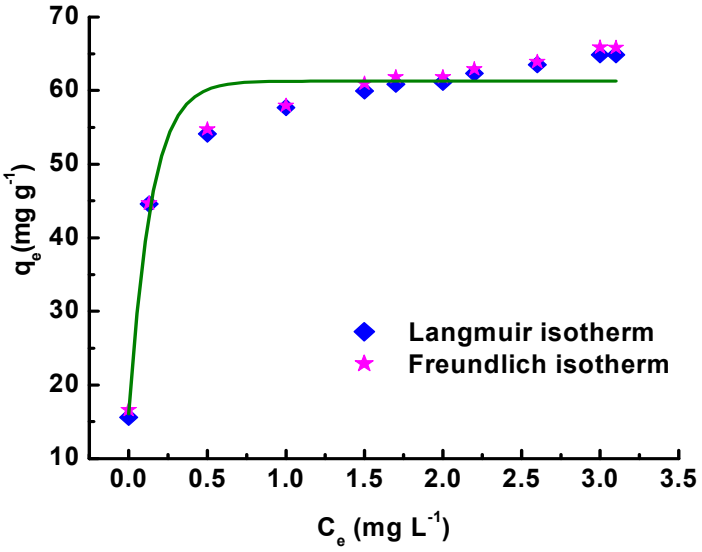

Fig. 8. Original Freundlich and Langmuir adsorption isotherms.

On comparing all the isotherm studies, the Freundlich and D–R isotherm provided the finest fit having a higher value of correlation coefficient, afterward, the Temkin and Langmuir isotherms.

Reaction kinetics

The mechanism of adsorption is described using a variety of kinetic models.[64,65] The irreversible nature of the adsorption is illustrated by using pseudo–first–order mathematical Equation 7.

$$\log(q_e - q_t) = \log q_e - (k_{ad}/2.303)t \quad (7)$$

where q_e and q_t signify the amount of fluoride adsorbed (mg g^{-1}) at equilibrium and at time 't', correspondingly and k_{ad} (min^{-1}) being the rate constant of pseudo–first–order reaction (Fig. S8†). The pseudo–second–order kinetic equation, signifying the chemisorption is shown in Equation 8.

$$t/q_t = 1/h + t/q_e \quad (8)$$

where 'h' signifies the rate constant for pseudo–second–order reaction.

From the linear kinetic plots, slope, and intercept were obtained (Fig. 9), and the kinetic parameters from them were determined, as tabulated in Table S3. A careful study of the data reveals that the pseudo–second–order model fitted better in the adsorption study having highest correlation coefficient ($R^2 > 0.982$). The intra–particle diffusion (Weber–Morris) expression is expressed by the following equation (Equation 9):

$$q_t = k_{id}\, t^{1/2} + C \quad (9)$$

where k_{id} is the intra–particle diffusion constant ((mg g $^{-1}$ min)$^{-(1/2)}$) and C is the intercept of the plot (Fig. S9†).[64] The rate of adsorption was very fast due to unsaturated sorption sites during the initial period of adsorption demonstrating intra–particle diffusion as rate–limiting step. This implies that intra–particle diffusion occurred first, which is a slow diffusion of fluoride ions from the surface site to the inside of the pores. Next to it, pseudo–second–order was the equilibrium rate–limiting step. Availability of free sites decreasing with time due to saturation making it difficult to carry on adsorption at fluoride saturated adsorbents.

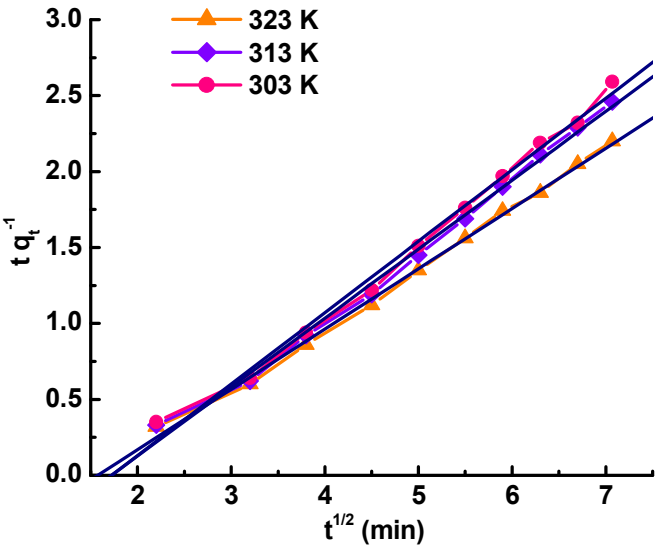

Fig. 9 The pseudo–second–order plots.

Thermodynamic studies

Temperature effect was studied at different temperatures and other optimal experimental conditions.[66] Thermodynamic parameters for instance standard free energy change (ΔG^0), standard enthalpy change (ΔH^0), and standard entropy change (ΔS^0) are described by Equations below (10−13):

$$\Delta G^0 = -2.303RT \log_{10} B_L \quad (10)$$

$$\log_{10}B_L(T_2) - \log_{10}B_L(T_1) = -(\Delta H^0/2.303R)[1/T_2 - 1/T_1] \quad (11)$$

$$\Delta H^0 = -\log_{10}B_L(T_2) - \log_{10}B_L(T_1) \times 2.303R/[1/T_2 - 1/T_1] \quad (12)$$

$$\Delta S^0 = (\Delta H^0 - \Delta G^0)/T \quad (13)$$

where ΔG^0 is free energy change (Kj mol^{-1}), where R is the universal gas constant (8.314 J mol^{-1} K^{-1}), T is the absolute temperature (K) and B_L is the Langmuir equilibrium constant, ΔH^0 is enthalpy change (kJ mol^{-1}), and ΔS^0 is entropy change (kJ mol^{-1}K^{-1}). The spontaneity

and endothermic nature of adsorption is supported by the negative and positive values of $\Delta G^0$and ΔH^0 , respectively (Table 2). The positive value of ΔS^0 proposed the increased entropy of the system during adsorption.[67] The increased disorder of system may also be due to changes in the hydration of adsorbing fluoride ions.

Table 2 Thermodynamic parameters' values of adsorbent at different temperatures

Parameter	Temperature (K)	Value
ΔG^0(kJ mol^{-1})	323	−1.746
	313	−1.803
	303	−0.766
ΔH^0(kJ mol^{-1})		+82.26
ΔS^0(J mol^{-1} K^{-1})		+277.24

Effect of pH and PZC

Results demonstrated that fluoride removal decreased on increasing pH above 6 and maximum was at pH 5 (Fig. 10). Out of specific and non–specific adsorption processes, specific adsorption happens due to ligand or anion exchange reactions which involve displacement of surface hydroxyl group by fluoride and columbic attraction occurs in non–specific adsorption.

However, it was observed (Fig. S10†) that maximum adsorption of fluoride was at pH 5 which is higher than the PZC of adsorbent (PZC = 4.5), which is indicating the utilization of specific and non–specific adsorption as confirmed by FTIR results. The removal mechanism in the acidic medium (pH 5), involving columbic attraction of fluoride by the surface positive charge is shown below in Equations 14 and 15.

$$MOH + H_2O + F^- \longrightarrow MOH_2^+ + F^- + OH^- \quad (14)$$

$$MOH_2 - F^- + OH^- \longrightarrow MF + H_2O + OH^- \quad (15)$$

It is apparent from Fig. 10 that the minimum adsorption occurs under both highly acidic and highly basic medium. In acidic pH range fluoride removal decreased as a result of the development of hydrofluoric acid (HF) as given in Equation 16.

$$H^+ + F^- \longrightarrow HF \quad (16)$$

Under alkaline condition, fluoride uptake diminished possibly as a result of electrical repulsion among negatively charged adsorbent surface sites. Additionally, fluoride ions competition for active surface sites with hydroxyl ions.[68]

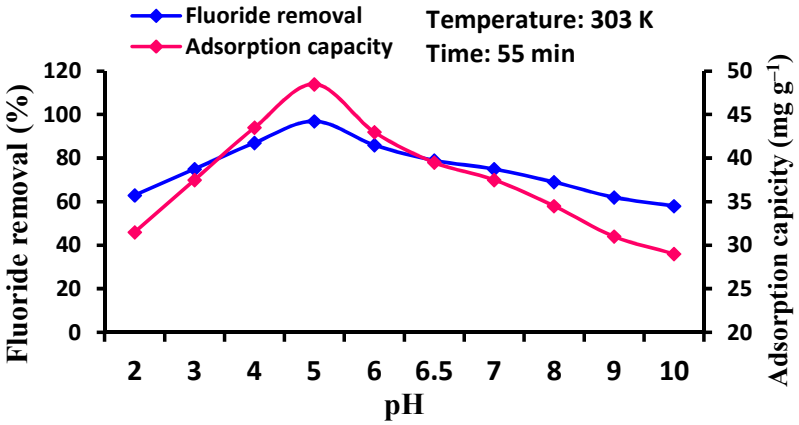

Fig. 10 Effect of pH.

Effect of adsorbent dose

It is apparent from Fig. 11 that the adsorption increases as the adsorbent dosage increases from 20–250 mg L^{-1}. This might be because of increase availability of active sites for adsorption which result in high removal efficiency.[69] However, additional raise in adsorbent dosage does not cause any significant fluoride removal as a result of adsorbent surface sites saturation. Thus, 220 mg L^{-1} is the best possible dose for adsorption.

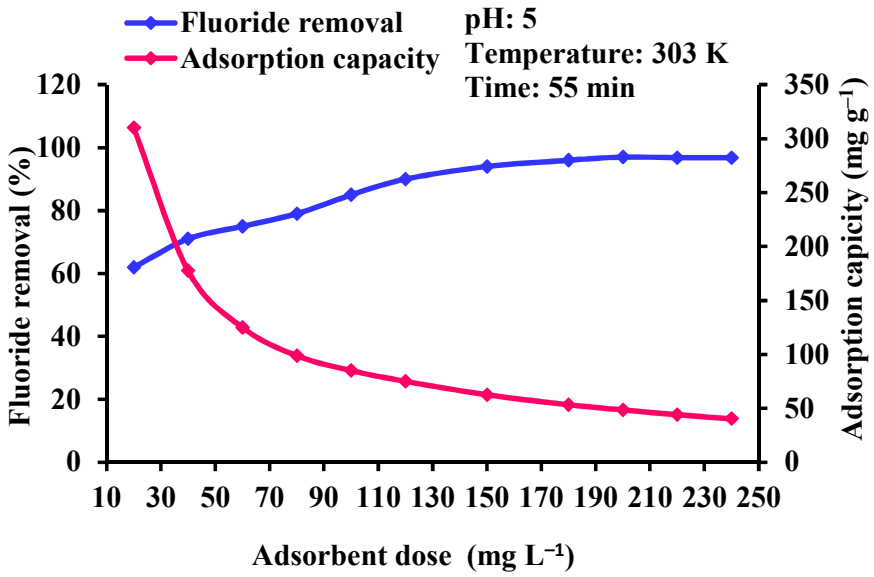

Fig. 11 Effect of adsorbent dose.

Effect of contact time

Adsorption behaviour was studied as a function of contact time from 5–80 min with the adsorbent dose 220 mg L^{-1}, pH 5 and temperature 303 K (Fig. 12). It had been confirmed that adsorption increased with time, and equilibrium was attained in 55 min. Fig. 12 shows that adsorption took place in three different phases. The initial phase indicates high adsorption occurs on unsaturated active sites. The second phase indicates a comparatively slow adsorption which is demonstrating utilization of the entire active sites over the adsorbent surface and achievement of saturation or equilibrium phase. The third and last phase indicates the equilibrium stage, which is showing a little adsorption as reported in the literature.[70,71]

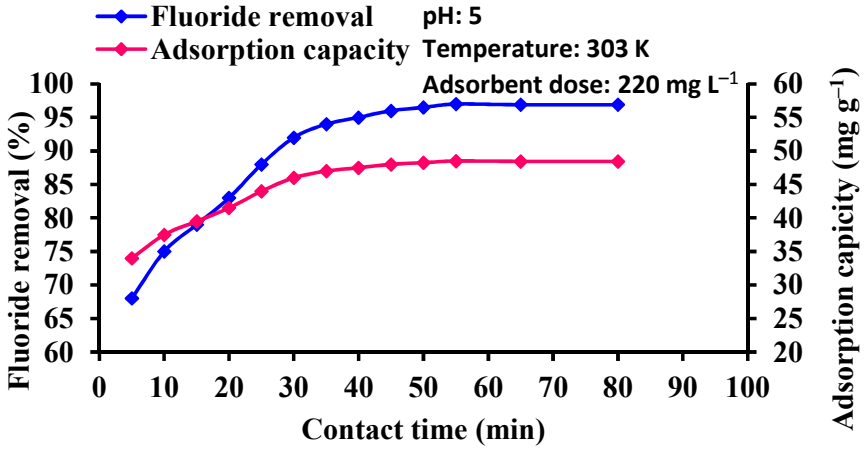

Fig. 12 Effect of contact time.

Effect of initial fluoride concentration

The adsorption was diminished with the initial fluoride concentration increased (Fig. 13). It can be explained as the competence of the adsorbent diminishes with augment of initial fluoride concentration. This is due to the fact that for a fixed adsorbent dose, the total accessible adsorption sites are restricted, and get saturated at a higher concentration as reported in literature.[72]

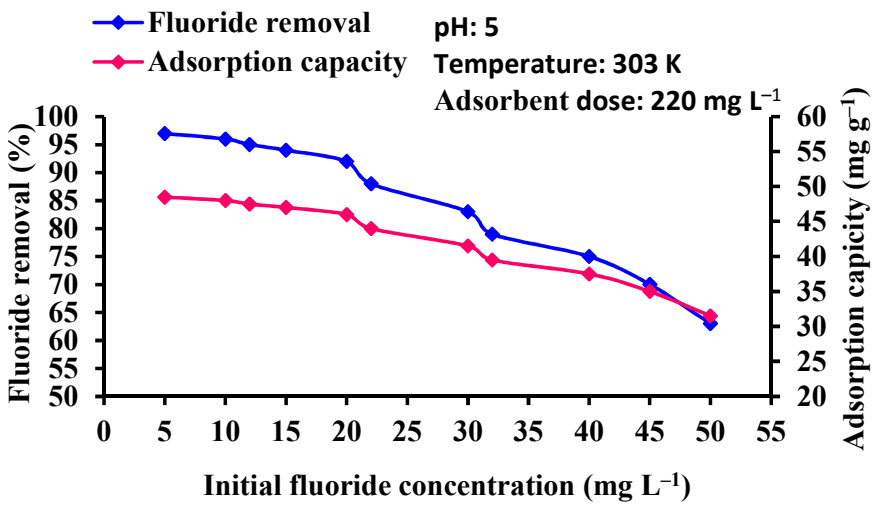

Fig. 13 Effect of initial fluoride concentration.

Effect of co–anions

Contaminated water contains a range of anions e.g. Cl^-, NO_3^-, SO_4^{2-}, CO_3^{2-}, HCO_3^-, and PO_4^{3-} in addition to F^- which may interfere in F^- adsorption as reported previously.[73] Fig. S11† shows that these anions have different effects with different concentrations on fluoride uptake. The presence of Cl^-, NO_3^-, SO_4^{2-}, CO_3^{2-}, and HCO_3^- had no significant effect on F^- removal even at elevated concentrations, possibly because of weak interactions with adsorbent surface sites. However, adsorption decreases rapidly as the concentration of PO_4^{3-} increases.[74] This may be due to increase in the negative electrical potential close to the adsorbent interface by phosphate ions which finally reduced the overall surface affinity for fluoride ions. Besides this, the larger sized phosphate anion may possibly obstruct adsorbent surface by this means diminishing the fluoride ions diffusing ability into adsorbent pores.

Comparative studies

Comparison of fluoride adsorption performance of a range of adsorbents is given in Table 3. Table 3 shows that the developed nanoadsorbent attained superior adsorption capacity than that of most previously reported adsorbents.

Table 3 Comparison of adsorption capacity of various adsorbents (from the Langmuir isotherm analysis)

Adsorbent	Initial F^- conc. (mg L^{-1})	pH	Adsorption capacity (mg g^{-1})	Reference
Fe–Ca–Ce nanoadsorbent	10–50	5.0	384.6	Present work
Quintinite	10–1,000	5.0–9.0	7.71	75
Mg/Al hydrotalcite–like	10–1,000	–	416.67	76
Mg/Al layered double hydroxides	100–200	4.0	4.14	77
Al–Ce hybrid adsorbent	1.0	12	27.5	78
treated biogenic apatite	3−80	5.0−6.0	360	79
nano–HA/chitin composite	10	7.0	150	80
nanoscale (AlOOH)	20	7.0	62.5	81
La alginate bead	–	4.0	197.2	82
Mn/Ce binary oxide	–	6.0	137.5	83

Desorption and reuse efficiency

The main purpose of the present study is to develop reusable, cost–effective and stable adsorbent. The desorption processes were performed on the nanoadsorbent by varying the pH using 0.1 M NaOH and re–activation was done with 0.1 M HCl. Fig. 14 shows that little desorption occurs at pH values lower than 8 and a maximum desorption of 90% occurs as the pH increases from 8–12. Reuse potential and the cycle stability of adsorbent were sufficiently high up to five cycles (Fig. S12†). The efficiency of the regenerated adsorbent decreased at the end of third cycle.

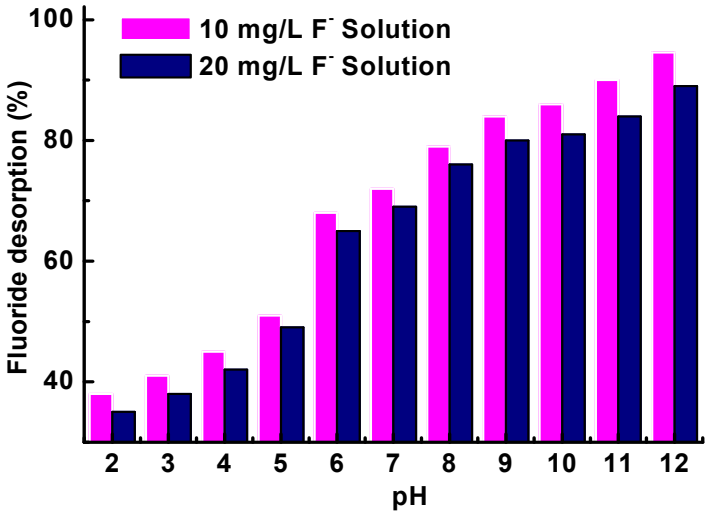

Fig. 14 Effect of solution pH on desorption.

Column studies

The untreated water had fluoride concentration of 8.0 mg L^{-1} which came down to a permissible limit (0.98 mg L^{-1}) after treatment indicates that the developed nanoadsorbent can be exploited in actual field conditions (Table 4). The influent water in column studies contained total bacterial population varying from 1.5×10^2 to 1.36×10^4 CFU 100 mL^{-1} with a mean of approximately 4.43×10^5 CFU 100 mL^{-1}. Following column treatment using nanoadsorbent, bacterial levels were decreased to an arithmetical mean of 1.4×10^2 CFU 100 mL^{-1}. Statistical analysis (t–test) demonstrated that the changes in bacterial levels were significantly different ($P < 0.0001$). Leaching test of the metal ions was performed using atomic absorption spectroscopy (AAS) analysis in treated water; no leached metal ions were detected which makes it sustainable adsorbent.

Table 4 Chemical quality of real water samples

Water quality parameter	Pre–treatment	Post–treatment
pH	8.73	8.31
EC (μS)	2548	2502
TDS (mg L^{-1})	401.0	324.0
DO (mg L^{-1})	5.70	5.30
F^- (mg L^{-1})	6.14	0.98

Cl^- (mg L^{-1})	250.0	213.0
PO_4^{3-} (mg L^{-1})	2.0	0.030
SO_4^{2-} (mg L^{-1})	350	193
CO_3^{2-} (mg L^{-1})	182	174
HCO_3^- (mg L^{-1})	204	196
NO_3^- (mg L^{-1})	40	28
NO_2^- (mg L^{-1})	1.5	1.10
Total coliform (CFU 100 mL^{-1})	4.43×10^5	1.4×10^2

Antibacterial activity studies

The concentration effect of nanomaterial on growth of *E. coli* is shown in Fig. S13† by determining optical density at 510 nm. The obtained data was compared with those of standard antibiotics in order to calculate the IC_{50} values (Figs. S13† and 15). T–test analysis presented $p < 0.005$ at higher nanomaterial concentration denoting significant difference from the control. It was found that 30 μg mL^{-1} concentration of nanomaterial inhibited the 50% growth of *E. coli* bacteria. Further the obtained IC_{50} value of nanomaterial was found comparable to those of standard antibiotics (Table 5). Additionally, the zone of inhibition (ZOI) developed by the nanomaterial was measured to be 27/30 mm. The ZOI of nanomaterial was found to be comparable to those of standard antibiotics viz. amoxicillin (28/31 mm), streptomycin (27/28 mm) demonstrating the effectiveness of nanomaterial as bactericidal agent (Fig. 16). The t–test presents large p value (> 0.05) signifying that there is no significant difference between the nanomaterials' and antibiotics' zone of inhibition (Fig. 17). Furthermore compared to previously accounted materials, the developed nanomaterial offered bigger zone of inhibition (Fig. 18).[84–86] An extensive antibacterial efficiency for Gram negative *E. coli* bacteria is possibly as a result of the interaction between the negative charge present on the bacterial outer membranes with nanomaterial. It has been found that outer membranes of *E. coli* bacteria are made up of lipopolysaccharides, which produced negative charge on the bacterial outer membranes and accordingly interact with the positive nanomaterial. Additionally, the high cationic nature of nanomaterial (MOH_2^+, pzc = 4.5) noticeably enhance its preferential recognition by the negative *E. coli* bacterial membranes.

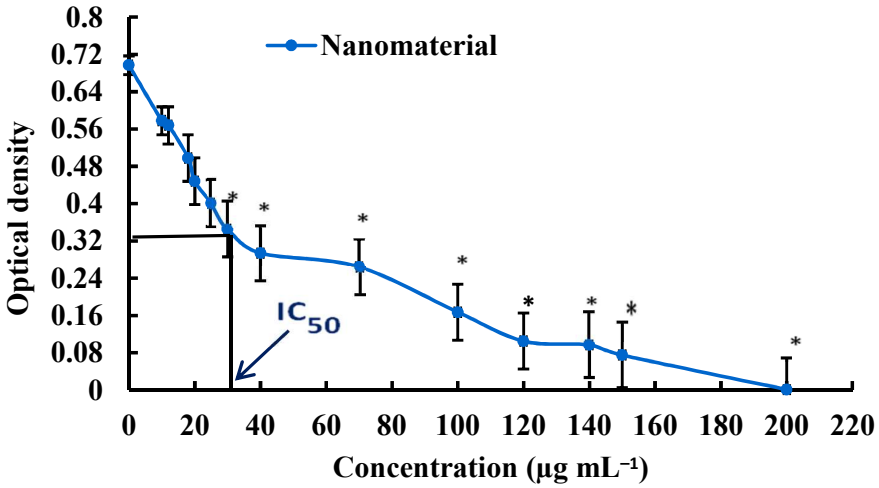

Fig. 15 UV–visible spectrophotometric calculation of IC_{50} values of nanomaterial. (mean ± SD of three independent experiments). Statistical significance was assessed by t–test and compared with controls (*) ($p < 0.005$).

Table 5 The IC_{50} values of standard antibiotics and nanomaterial

Sample	IC_{50} (μg mL^{-1})
Amoxicillin	9.5
Streptomycin	9.7
Nanomaterial	30.0

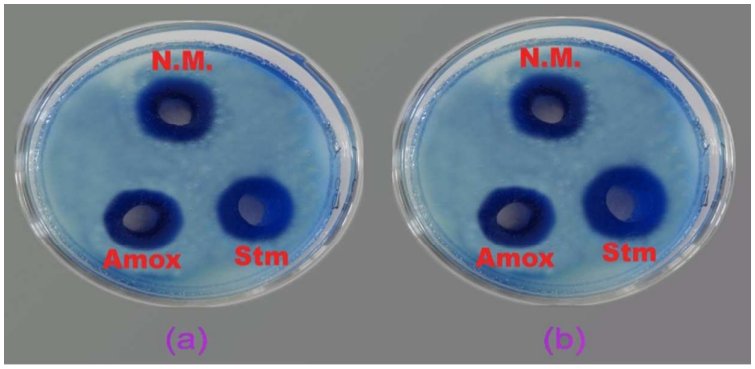

Fig. 16 Zone of inhibition (mm) generated by the nanomaterial and standard antibiotics.

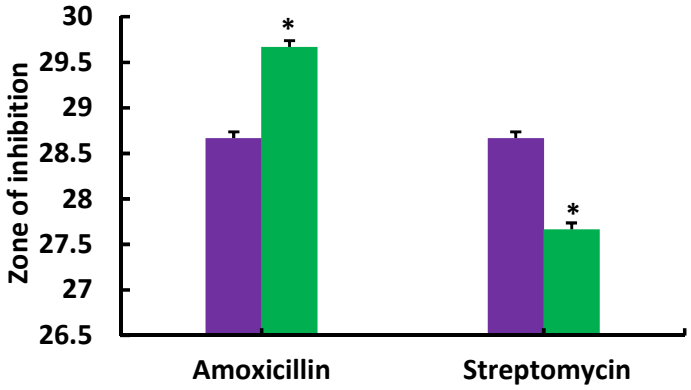

Fig. 17 Comparable zone of inhibition (mm) by nanomaterial and antibiotics, purple column shows zone of inhibition by nanomaterial (mean ± SD of three independent experiments). For antibiotics' zone of inhibition, an asterisk (*) denotes that there is no significant difference from the nonamaterial's zone of inhibition consistent with a t–test ($p > 0.05$).

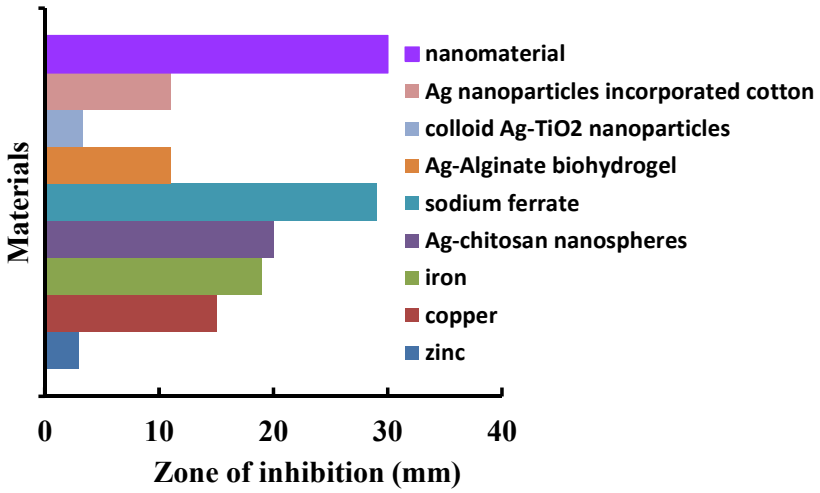

Fig. 18 Comparative zone of inhibition of developed nanomaterial and different materials against *E. coli.*

Effect of nanoadsorbent on membrane protein leakage

In control experiment, almost 7.60 μg mg^{-1} of protein leakage was detected from bacterial cells, whereas 8.89 μg mg^{-1} of protein from cells (Fig. 19) leaked with nanomaterial (100 μg mL^{-1}) treatment. After 4 h of treatment with nanomaterial, the leakage amount of protein was found to be up to 15.5 μg mg^{-1}, but it was only 10.30 μg mg^{-1} in control experiment, signifying the effect of nanomaterial on protein leakage acceleration from bacterial cytoplasm. The calculated p value (t = 4 h, $p < 0.03$) for protein leakage was smaller than initial (t = 0 h, $p < 0.05$) indicating significant difference from the control. Interestingly a sub

lethal nanomaterial concentration (50 μg mL^{-1}), caused enhancement in the inner membrane permeability of bacteria. Further, increased nanomaterial concentration caused the enhanced leakage of large cytoplasmic protein components, causing the death of bacteria. Accordingly, it can be speculated that high nanomaterial concentration caused rapid killing of bacteria by extreme loss of membrane integrity.

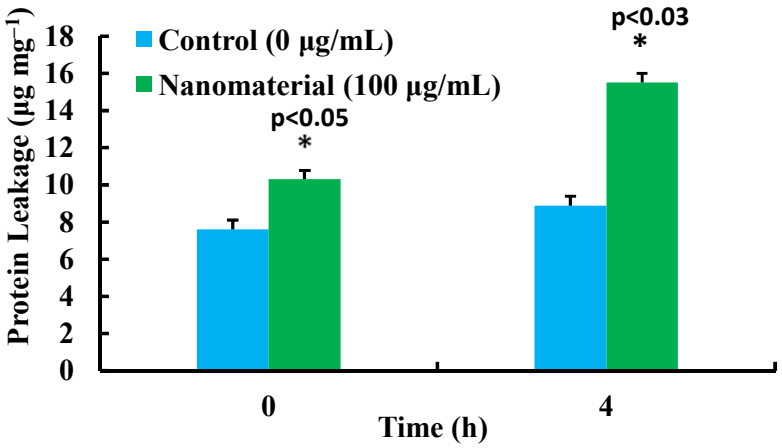

Fig. 19 Protein leakage analysis of nanomaterial (mean ± SD of three independent experiments), where, an asterisk (*) designates the significant difference from the control in accordance with t–test ($p < 0.05$).

Effect of nanomaterial on dehydrogenases enzyme activity

It was found that the activity of enzyme in control (+) *E. coli* cells enhanced, whereas the enzymatic activity in control (−) cells remained almost unchanged with the incubation time (Fig. 20). Initially, the activity of cell's enzyme with 100 μg mL^{-1} nanomaterial concentration was superior to that of control (+), but it decreased quickly with an increase in incubation period. The enzymatic activity decreased instantly after 5 min with 100 μg mL^{-1} nanomaterial concentration and maintained a low activity for 30 min during treatment. Therefore, it can be inferred that the dehydrogenases enzyme activity of *E. coli* was found to be inhibited by nanomaterial, and can be directly related to the concentration of nanomaterial. Therefore, it is assumed that nanomaterial broke the outer membrane barrier and damaged dehydrogenases enzyme activity (Fig. 20).

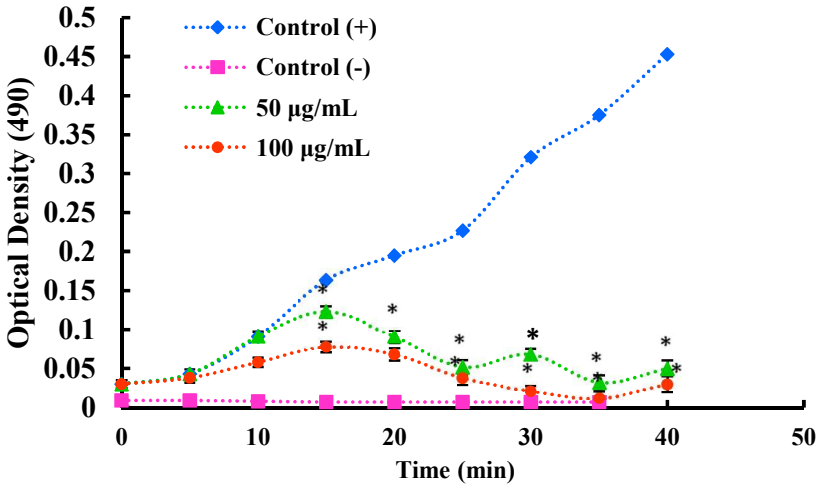

Fig. 20 Effect of nanomaterial on dehydrogenase enzyme activity in *E. coli* cells (mean ± SD of three independent experiments), where control (−) and control (+) represent the boiled and not boiled *E. coli* cells, respectively. Where, statistical analysis was calculated by t–test and compared with controls (*).

Conclusions

The adsorbent performed well within pH range of 5.0–6.0, with high removal ability. Kinetic data fitted well to pseudo–second–order kinetic model. The adsorption isotherm followed Freundlich and D–R isotherm models well. Thermodynamic investigation illustrated endothermic as well as spontaneous nature of fluoride uptake with the increase of entropy of the system. Other co–anions such as SO_4^{2-}, CO_3^{2-}, Cl^- HCO_3^- , NO_3^-, but not PO_4^{3-} had no considerable effect on adsorption efficiency. Additionally, the advantage of nanoadsorbent in treating real water samples and no leach out effect makes it more attractive towards fluoride uptake. The adsorbent retained a considerable adsorption capacity even after three complete adsorption–desorption cycle, confirming the reusability of the nanoadsorbent. The antibacterial activity experiments results indicated excellent IC_{50} value (30 μg mL^{-1}) and demonstrated 27/30 mm zone of inhibition. Treatment with nanomaterial induced cell's proteins leakage and also induced the inactivity of dehydrogenase enzyme, signifying the potential ability of nanomaterial to destroy *E. coli* cells.

Acknowledgment

We gratefully acknowledge support from the Ministry of Human Resource Development Department of Higher Education, Government of India under the scheme of Establishment of

Centre of Excellence for Training and Research in Frontier Areas of Science and Technology (FAST), for providing the necessary financial support to carry out this study vide letter No, F. No. 5–5/201 4–TS.Vll.

References

1. S. Samatya, U. Yuksel, M. Yuksel and N. Kabay, *Sep. Sci. Technol.,* 2007, **42**, 2033.
2. Z. Mandinic, M. Curcic, B. Antonijevic, M. Carevic, J. Mandic, D. Djukic–Cosic and C. P. Lekic, *Sci. Total Environ.,* 2010, **408**, 3507.
3. N. Gandhi, D. Sirisha, S. Asthana and A. Manjusha, *Res. J. Chem. Sci.,* 2012**, 2**, 32.
4. B. F. Gooch, DMD, MPH, Centers for Disease Control and Prevention, Public health service recommendation for fluoride concentration in drinking water for the prevention of dental caries, National Center for Chronic Disease Prevention and Health Promotion, Division of Oral Health, 4770 Buford Hwy. NE, MS F–80, Atlanta, GA 30341–3717, U.S. Public Health Reports, 2015, 130, 1.
5. H. W. Khandare, *Int. J. Chem. Tech. Res.,* 2013, **5**, 502.
6. S. P. Teotia and M. Teotia, *Jour. Asso. Physicians India*, 1994, **32**, 347.
7. Meenakshi and R. C. Maheshwari, *J. Hazard. Mater.,* 2006, **137**, 456.
8. A. Tor, N. Danaoglu, G. Arslan and Y. Cengeloglu, *J. Hazard. Mater.,* 2009, **164**, 271.
9. N. I. Chubar, V. F. Samanidou, V. S. Kouts, G. G. Gallios, V. A. Kanibolotsky, V. V. Strelko and I. Z. Zhuravlev, *J. Colloid Interface Sci.,* 2005, **291**, 67.
10. M. G. Sujana, R. S. Thakur, S. N. Das and S. B. Rao, *Asian J. Chem.,* 1997, **9**, 561.
11. M. Hichour, F. Persin, J. Sandeaux and C. Gavach, *Sep. Purif. Technol.,* 2000, **18**, 1.
12. N. Kabay, O. Arar, S. Samatya, U. Yuksel and M. Yuksel, *J. Hazard. Mater.,* 2008, **153**, 107–113.
13. S. Sourirajan and T. Matsurra, *Water Res.,* 1972**, 6**, 1073.
14. R. Simons, *Desalination,* 1993**, 89**, 325.
15. L. Guo, B. J. Hunt and P. H. Santsci, *Water Res.,* 2001, **35**, 1500.
16. M. S. Onyango, H. Matsuda and T. Alain, *Adv. Fluorine Sci.,* 2006, **2**, 1.
17. M. A. M. Sahli, S. Annouar, M. Tahaikt, M. Mountadar, A. Soufiane and A. Elmidaoui, *Desalination,* 2007**, 212**, 37.
18. X. Liao and B. Shi, *Environ. Sci. Technol.,* 2005, **39**, 4628.
19. A. Bhatnagar, E. Kumar and M. Sillanpa, *Chem. Eng. J.,* 2011, **171**, 811.
20. V. Ganvir and K. Das, *J. Hazard. Mater.,* 2011, **185**, 1287.

21. A. A. M. Daifullah, S. M. Yakout and S. A. Elreefy, *J. Hazard. Mater.,* 2007, **147**, 633.
22. N. A. Medellin–Castillo, R. Leyva–Ramos, R. Ocampo–Perez, R. F. de la Cruz, A. Aragon–Pina and J. M. Martinez–Rosales, *Ind. Eng. Chem. Res.,* 2007, **46**, 9205.
23. N. Viswanathan and S. Meenakshi, *J. Hazard. Mater.,* 2009, **162**, 920.
24. L. Lv, J. He, M. Wei, D. G. Evans and Z. L. Zhou, *Water Res.,* 2007, **41**, 1534.
25. S. Meenakshi, C. S. Sundaram and R. Sukumar, *J. Hazard. Mater.,* 2008, **153**, 164.
26. N. Viswanathan, C. S. Sundaram and S. Meenakshi, *J. Hazard. Mater.,* 2009, **161**, 423.
27. A. Bansiwal, D. Thakre, N. Labhshetwar, S. Meshram and S. Rayalu, *Colloids Surf. B,* 2009, **74**, 216.
28. S. Lunge, R. Biniwale, N. Labhsetwar and S. S. Rayalu, *J. Hazard. Mater.,* 2011, **191**, 325.
29. A. Tor, *Desalination,* 2006, **201**, 267.
30. V. E. Badillo–Almaraz, J. A. Flores, H. Arriola, F. A. Lopez and L. Ruiz–Ramirez, L. *J. Radioanal. Nucl. Chem.,* 2007, **271**, 741.
31. X. Fan, D. J. Parker and M. D. Smith, *Water Res.,* 2003, **37**, 4929.
32. B. D. Turner, P. Binning and S. L. S. Stipp, *Environ. Sci. Technol.,* 2005, **39**, 9561.
33. Y. Zhang, X. M. Dou, M. Yang, H. He, C. Y. Jing and Z. Y. Wu, *J. Hazard. Mater.,* 2010, **179**, 208.
34. X. Wu, Y. Zhang, X. Dou and M. Yang, *Chemosphere,* 2007, **69**, 1758.
35. V. Kumar, N. Talreja, D. Deva, N. Sankararamakrishnan, A. Sharma and N. Verma *Desalination,* 2011, **282**, 27.
36. K. Biswas, S. K. Saha and U. C. Ghosh, *Chem. Eng. J.,* 2009, **149**, 196.
37. K. Biswas, S. K. Saha and U. C. Ghosh, *Desalination,* 2010, **255**, 44.
38. L. Chen, T. J. Wang, H. X. Wu, Y. Jin, Y. Zhang and X. M. Dou, *Powder Technol.,* 2011, **206**, 291.
39. H. Liu, S. B. Deng, Z. J. Li, G. Yu and J. Huang, *J. Hazard. Mater.,* 2010, **179**, 424.
40. V. Sivasankar, S. Murugesh, S. Rajkumar and A. Darchen, *Chem. Eng. J.,* 2013, **214**, 45.
41. J. L. Sedillo, A. Quintana, K. Sousa, K. H. Oshima and G. B. Smith, *J. Environ. Monit.,* 2008, **10**, 718.
42. L. C. Gerber, N. Moser, N. A. Luechinger, W. J. Stark and R. N. Grass, *Chem. Commun.,* 2012, **48**, 3869.

43. A. Fujishima, T. N. Rao and D. A. Tryk, *J. Photochem. Photobiol. C,* 2000, **1**, 1.
44. J. V. D. Vossenberg, H. Tervahauta, K. Maquelin, C. H. W. B. Koopmans, M. U. Aarts, D. V. D. Kooij, A. P. V. Wezel and B. V. D. Gaag, *Anal. Methods,* 2013, **5**, 2679.
45. C. Lee, J. Y. Kim, W. I. Lee, K. L. Nelson, J. Yoon and D. L. Sedlak, *Environ. Sci. Technol.*, 2008, **42**, 4927.
46. D. Guin, S. V. Manorama, J. N. L. Latha and S. Singh, *J. Phys. Chem. C,* 2007, **111**, 13393.
47. A. Dhillon and D. Kumar, *J. Mater. Chem. A,* 2015, **3**, 4215.
48. M. M. Bradford, *Anal. Biochem.,* 1976, **72**, 248.
49. P. R. Twentyman and M. Luscombe, *Br. J. Cancer.,* 1987, **56**, 279.
50. S. Brunauer, P. H. Emmett and E. Teller, *J. Am. Chem. Soc.,* 1938, **60**, 309.
51. A. Gil, S. A. Korili and G. Y. Cherkashinin, *J. Colloid Interface Sci.,* 2003, **262**, 603.
52. J. D. Russell, *Clay Miner.,* 1979, **14**, 109.
53. M. G. Sujana and S. Mohanty, *Int. J. Eng. Sci.,* 2010, **2**, 1.
54. B. Pan, J. Xu, B. Wu, Z. Li, and X. Liu, *Environ. Sci. Technol.,* 2013, **47**, 9347.
55. T. Ahmad, S. Khatoon, S. E. Lofland and G. S. Thakur, *Mater. Sci. Semicond. Process.,* **2014**, 17, 207.
56. H. S. Jabur, *Journal of Thi–Qar University,* 2008, **4**, 27.
57. T. Zhang, Q. Li, H. Xiao, Z. Mei, H. Lu and Y. Zhou, *Appl. Clay Sci.* 2013, **72**, 117.
58. M. Kovácsa, Z. Valicsek, J. Tóthc, L. Hajba, É. Makód, P. Halmos and R. Földényi, *Colloids and Surfaces A: Physicochem. Eng. Aspects,* 2009, **352**, 56.
59. D. A. Kumar, S. Selvasekarapandian, H. Nithya, and Y. Masuda, *Solid State Sci.,* 2012, **14**, 626.
60. D. L. Clark, J. C. Gordon, P. J. Hay, and R. Poli, *Organometallics,* 2005**, 24***,* 5747.
61. G. Zhang, Z. He and W. Xu, *Chem. Eng. J.,* 2012, **183**, 315.
62. K. Vijayaraghavan, T. V. N. Padmesh, K. Palanivelu and M. Velan, *J. Hazard. Mater.,* 2006, **133**, 304–308.
63. M. Islam and R. K. Patel, *J. Hazard. Mater.,* 2007, **143**, 303.
64. S. K. Swain, S. Mishra, T. Pattnaik, R. K. Patel, U. Jha and R. K. Dey, *Chem. Eng. J.,* 2012, **184**, 72.
65. Y. S. Ho and G. McKay, *Process Biochem.,* 1999, **34**, 451.
66. M. H. Jnr and Spiff, *Electron. J. Biotechnol.,* 2005, **8**, 162.
67. N. Viswanathan, S. M. Prabhu and S. Meenakshi, *J. Fluorine Chem.,* 2013, **153**, 143.

68. S. Chakrabortty, M. Roy and P. Pal, *Desalination,* 2013, **313**, 115.
69. S. Gao, R. Sun, Z. Wei, H. Zhao, H. Li and F. Hua, *J. Fluorine Chem.,* 2009, **130**, 550.
70. M. Srimurali, A. Pragathi and Karthikeyan, *J. Environ. Pollut.,* 1998, **99**, 285.
71. S. V. Ramanaiah, S. V. Mohan and P. N. Sarma, *Ecol. Eng.,* 2007, **31**, 47.
72. S. Chakrabarty and H. P. Sarma, *Int. J. Chem. Tech. Res.* 2012, **4**, 511.
73. J. Liu, L. Wan, L. Zhang and Q. Zhou, *J. Colloid Interface Sci.,* 2011, **364**, 490.
74. D. Thakre, S. Jagtap, N. Sakhare, N. Labhsetwar, S. Meshram and S. Rayalu, *Chem. Eng. J.,* 2010, **158**, 315.
75. J. H. Kim, J. A. Park, J. K. Kang, J. W. Son, I. G. Yi and B. Kim, *Environ. Eng. Res.,* 2014, **19**, 247.
76. S. Mandal and S. Mayadevi, *J. Hazard. Mater.,* 2009, **167**, 873.
77. J. H. Kim, C. G. Lee, J. A. Park, J. K. Kang, S. Y. Yoon and S. B. Kim, *Water Sci. Technol. Water Supply,* 2013, **13**, 249.
78. H. Wang, J. Chen, Y. Cai, J. Ji, L. Liu and H. H. Teng, *Appl. Clay Sci*., 2007, **35**, 59.
79. S. Gao, J. Cui and Z. G. Wei, *J. Fluorine Chem.,* 2009, **130**, 1035.
80. C. S. Sundaram, N. Viswanathan and S. Meenakshi, *J. Hazard. Mater.,* 2009, **172**, 147.
81. F. Adeno, E. Mulugeta, F. Zewge and Y. Chebude. *Bull. Chem. Soc. Ethiop.,* 2014, **28**, 215.
82. Y. Huo, W. Ding, X. Huang, J. Xu and M. Zhao, *Chin. J. Chem. Eng.,* 2011, **19**, 365.
83. S. Deng, H. Liu, W. Zhou, J. Huang and G. Yu, *J. Hazard. Mater.,* 2011, **186**, 1360.
84. P. K. Tandon, S. B. Singh and R. C. Shukla, *Ind. Eng. Chem. Res.,* 2013**, 52**, 17038.
85. A. Azam, A. S. Ahmed, M. Oves, M. S. Khan, S. S. Habib and A. Memic, *Int. J. Nanomedicine,* 2012, **7**, 6003.
86. P. Singh, J. Bajpai, A. K. Bajpai and R. B. Shrivastava, *Indian J. Chem. Technol.,* 2011, **18**, 403.

Table of Contents (TOC)

Highly cationic tri–metal oxide (Fe-Ca-Ce) based nanomaterial for excellent fluoride decontamination and bactericidal efficiency.